International Journal of Nanomedicine

Dovepress
open access to scientific and medical research

Open Access Full Text Article

ORIGINAL RESEARCH

Enhanced and Prolonged Antitumor Effect of Salinomycin-Loaded Gelatinase-Responsive Nanoparticles via Targeted Drug Delivery and Inhibition of Cervical Cancer Stem Cells

This article was published in the following Dove Press journal:
International Journal of Nanomedicine

Qin Wang,[1,*] Fangcen Liu,[2,*] Lifeng Wang,[1] Chen Xie,[3] Puyuan Wu,[1] Shiyao Du,[1] Shujuan Zhou,[1] Zhichen Sun,[1] Qin Liu,[1] Lixia Yu,[1] Baorui Liu,[1] Rutian Li[1]

[1]The Comprehensive Cancer Centre of Drum Tower Hospital, Medical School of Nanjing University, Clinical Cancer Institute of Nanjing University, Nanjing 210008, People's Republic of China; [2]The Comprehensive Cancer Centre, Nanjing Drum Tower Hospital, Clinical College of Nanjing Medical University, Nanjing, People's Republic of China; [3]Key Laboratory for Organic Electronics and Information Displays, Institute of Advanced Materials (IAM), Jiangsu National Synergetic Innovation Center for Advanced Materials (SICAM), Nanjing University of Posts & Telecommunications, Nanjing 210023, People's Republic of China

*These authors contributed equally to this work

Correspondence: Rutian Li; Baorui Liu
The Comprehensive Cancer Centre of Drum Tower Hospital, Medical School of Nanjing University, Clinical Cancer Institute of Nanjing University, 321 Zhongshan Road, Nanjing 210008, People's Republic of China
Tel +86-25-83107081
Fax +86-25-83317016
Email rutianli@nju.edu.cn; baoruiliu@nju.edu.cn

Background: Cervical cancer stem cells (CCSCs) represent a subpopulation of tumor cells that possess self-renewal capacity and numerous intrinsic mechanisms of resistance to conventional chemotherapy and radiotherapy. These cells play a crucial role in relapse and metastasis of cervical cancer. Therefore, eradication of CCSCs is the primary objective in cervical cancer therapy. Salinomycin (Sal) is an agent used for the elimination of cancer stem cells (CSCs); however, the occurrence of several side effects hinders its application. Nanoscale drug-delivery systems offer great promise for the diagnosis and treatment of tumors. These systems can be used to reduce the side effects of Sal and improve clinical benefit.

Methods: Sal-loaded polyethylene glycol-peptide-polycaprolactone nanoparticles (Sal NPs) were fabricated under mild and non-toxic conditions. The real-time biodistribution of Sal NPs was investigated through non-invasive near-infrared fluorescent imaging. The efficacy of tumor growth inhibition by Sal NPs was evaluated using tumor xenografts in nude mice. Flow cytometry, immunohistochemistry, and Western blotting were used to detect the apoptosis of CSCs after treatment with Sal NPs. Immunohistochemistry and Western blotting were used to examine epithelial–mesenchymal transition (epithelial interstitial transformation) signal-related molecules.

Results: Sal NPs exhibited antitumor efficacy against cervical cancers by inducing apoptosis of CCSCs and inhibiting the epithelial–mesenchymal transition pathway. Besides, tumor pieces resected from Sal NP-treated mice showed decreased reseeding ability and growth speed, further demonstrating the significant inhibitory ability of Sal NPs against CSCs. Moreover, owing to targeted delivery based on the gelatinase-responsive strategy, Sal NPs was more effective and tolerable than free Sal.

Conclusion: To the best of our knowledge, this is the first study to show that CCSC-targeted Sal NPs provide a potential approach to selectively target and efficiently eradicate CCSCs. This renders them a promising strategy to improve the therapeutic effect against cervical cancer.

Keywords: nanoparticles, salinomycin, tumor-targeted delivery, cancer stem cells, epithelial interstitial transformation

Introduction

Cervical cancer (CC) is the fourth most common cancer in women worldwide,[1,2] with an estimated 570, 000 new cases and 41,000 CC-related deaths annually.[3] Since the introduction of formal screening programs, the rates of CC among women

in high-income countries have been decreasing; however, they remain high among those in low- and middle-income countries that lack organized screening and human papillomavirus infection vaccination programs.[4] Effective treatments for patients with early-stage CC include surgical resection and concurrent chemoradiotherapy,[5] which can result in a 5-year survival of ≤80%. For locally advanced CC, the 5-year survival rates of stage IIB, IIIA, and IIIB disease vary (58%, 35%, and 32%, respectively).[6] However, 30–50% of patients ultimately develop tumor recurrence and metastasis,[6] which impairs the long-lasting, effective treatment of CC.[7,8] For this subset of patients, systemic chemotherapy remains the cornerstone of treatment. Notably, the combination of bevacizumab with platinum-based chemotherapy, can improve median overall survival by 3.5 months compared with chemotherapy alone (16.8 vs 13.3 months, respectively).[9,10] Pembrolizumab, an inhibitor of Programmed cell death 1 protein (PD-1), has received approval by the US Food and Drug Administration for the treatment of advanced CC with progressive disease. Although targeted therapy and immunotherapy have shown some survival advantages in the treatment of patients with recurrent and metastatic disease, the cost and affordability limit their use for patients in low- and middle-income countries.[11,12] Thus, there is an urgent need to develop novel and more effective strategies for the treatment of CC patients with progressive disease.

Cancer stem cells (CSCs) are pluripotent cells, which account for a small proportion of cells within numerous types of tumors or cancer cell lines. They exhibiting great capability for differentiation into progeny of malignant cells and are less sensitive to regular therapies, such as radiotherapy and chemotherapy.[13,14] Cervical cancer stem cells (CCSCs) are recognized as the "seed" for cancer metastasis and relapse.[15] They were first isolated using the spheroid method, are characterized as highly tumorigenic and radioresistant, and possess self-renewal properties.[16] In another report, CCSCs were also associated with tumor invasion, chemoresistance, and epithelial–mesenchymal transition (EMT).[17] Moreover, CCSCs play an important role in tumor heterogeneity, which is associated with a poor response to chemotherapy/radiotherapy, carcinogenesis, metastasis, and recurrence.[8,18,19] Therefore, the development of novel therapeutic strategies specifically targeting CCSCs is urgently warranted to eliminate the cancer "seed."

Salinomycin (Sal) is a polyether antibiotic isolated from *Streptomyces albus*. In 2009, Gupta et al first demonstrated that Sal reduced the proportion of breast CSCs by >100 fold relative to paclitaxel.[20] Since then, Sal has been reported as an effective anti-cancer drug against various types of CSCs, such as those of colorectal cancer, pancreatic cancer, and prostate cancer.[21–23] It can inhibit the maintenance of CSCs by promoting their differentiation and sensitivity to chemotherapy and radiotherapy.[24–27] Hence, we hypothesized that Sal may also be useful in inhibiting CCSCs. However, severe nerve and muscle toxicity, and even death in humans after accidental oral or inhaltive intake of Sal have been reported.[28–30] In addition, the applications of Sal are limited due to its poor aqueous solubility.[31] Thus, delivery systems have attracted considerable attention owing to their excellent performance and favorable characteristics, such as ameliorating the inapplicable properties of drugs or pharmacokinetic properties.[32] Moreover, enhanced accumulation of drug at the tumor site via the enhanced permeability and retention effect (EPR) can improve the safety and tolerability of drugs, thereby achieving significant clinical benefit with attenuated side effects.[33] Modification of nanoparticles (NPs) with polyethylene glycol (PEGylation) can strengthen the EPR effect-mediated "passive" tumor targeting, leading to prolonged circulation of NPs in the blood.[34] In addition to passive targeting, active targeting drug delivery can be achieved by surface modification with tumor target ligands or engineering with microenvironment-stimulus responsive characteristics.[35]

Matrix metalloproteinases (MMPs) represent a family of zinc-dependent endopeptidases that play important roles in cancer invasion, metastasis, angiogenesis, and tumorigenesis.[36,37] MMPs can degrade the extracellular matrix, which is overexpressed and overactivated in cancer.[38] Furthermore, three MMP family members (i.e., MMP2, MMP7, and MMP14) are known to induce EMT progression in different types of cancer.[39,40] Thus, MMPs have been investigated as robust tumor microenvironmental stimuli for "smart" MMP-responsive drug delivery and tumor targeting, and have shown great potential in the diagnosis and therapy of cancer. Based on this evidence, we generated gelatinase-stimuli NPs. These are modified by inserting an optimal gelatinase-cleavable peptide Pro-Val-Gly-Leu-Iso-Gly (PVGLIG) into non-toxic, biocompatible PEG-polycaprolactone (PEG-PCL) copolymer, and can more specifically target CSCs. We have already developed a novel and biocompatible nanocarrier to deliver Sal to CC and confirmed the optimal parameters for the preparation of

Sal NPs.[27] The poor aqueous solubility of Sal can be overcome by our Sal NPs, yielding an encapsulation efficiency of 89.7%. Preliminary toxicity observation indicated a strikingly higher survival rate in mice injected with Sal-loaded NPs than Sal Free treated group. These results demonstrated that entrapment of Sal into NPs prepared through the single emulsion method greatly reduced the occurrence of toxic effects. In this study, we successfully prepared Sal NPs using this approach. The present investigation outlines the safety profile, anti-tumor efficacy, and inhibitory activity of Sal NPs against CSCs.

Materials and Methods

Materials

Methoxy-PEG (mPEG)-peptide-PCL copolymer was prepared in our laboratory as previously described;[41] Sal was purchased from the China Institute of Veterinary Drug Control (Beijing, China). Human CD44 and CD133 antibodies were purchased from Miltenyi Biotec (Germany) and human vimentin (VIM), E-cadherin, zinc finger E-box binding homeobox 1 (ZEB1), and ZEB2 antibodies were purchased from Abcam (USA). All other chemicals were used as received without further treatment. The liVision plus kit and DAB kit were purchased from Fuzhou New Biotechnology Co., Ltd. (Fuzhou, China). The total protein extraction kit, sodium dodecyl sulfate-polyacrylamide gel electrophoresis, Western blotting (WB) testing kit, enhanced chemiluminescence testing kit, and Braford protein testing kit were purchased from Nanjing KeyGEN Biotech. Co., Ltd. (Nanjing, China).

Cell Lines and Culture

HeLa, a highly metastatic human cell line, was purchased from the Shanghai Institute of Biochemistry and Cell Biology, (Shanghai, China). The cells were cultivated in Rosewell Park Memorial Institute (RPMI) 1640 medium, supplemented with 10% fetal bovine serum and incubated at 37°C in a humidified chamber containing 5% CO_2.

Real-Time Near-Infrared Fluorescent (NIRF) Imaging

The real-time biodistribution of Sal NPs was investigated through non-invasive NIRF imaging. Sal NPs were labeled with NIR-797-isothiocyanate (Sigma–Aldrich) to track the position of particles. Briefly, the NIR-797-isothiocyanate and mPEG-peptide-PCL copolymers were dissolved in dimethylformamide and stirred at room temperature for 18 h. After the reaction, unconjugated NIR-797-isothiocyanate was removed via dialysis (MWCO 3500 Da) for 2 days. The NIR-797-labeled NP solution was lyophilized for further use.

A total of 10^7 HeLa tumor cells were subcutaneously inoculated into the right posterior flanks of male BALB/c nude mice (age: 5–6 weeks, weight: 18–22 g) to establish the tumor model. The NIR-797-labeled Sal NPs (equivalent to the dose of Sal 2 mg/kg in an antitumor study) were administered through intraperitoneal (IP) injection into HeLa tumor-bearing mice (the same tumor model for the following antitumor study) on day 7 after inoculation. The real-time biodistribution image of NPs in tumor-bearing mice was captured using the IVIS® Lumina system (Xenogen Co., Alameda, CA, USA) at 1, 24, 48, 72, 96, and 120 h post administration. The NIRF at 745 nm was collected and the exposure time was set to 2 s.

In vivo Antitumor Effect of Sal NPs

Male BALB/c nude mice (age: 4–5 weeks, weight: 18–22 g) purchased from the Animal Care Committee at Drum Tower Hospital (Nanjing, China) were housed under specific-pathogen-free (SPF) conditions and allowed to acclimatize to the laboratory conditions for 1 week prior to initiating the experiment. All animal studies were performed in compliance with guidelines established by the Animal Care Committee at Drum Tower Hospital, Nanjing, China. The Animal Care Committee at Drum Tower Hospital approved the experiments.

Ten male BALB/c nude mice (age: 4–5 weeks, weight: 18–22 g), housed under SPF conditions were subcutaneously injected at the lower right axilla with 0.1 mL of cell suspension containing 10^7 HeLa CC cells. The mice whose tumor reached approximately 500 mm^3 were sacrificed. The tumors were cut into pieces (3 × 3 × 3 mm). Tumor pieces were subcutaneously implanted on the right axilla of BALB/c nude mice. When tumor volumes reached approximately 100–200 mm^3, the mice were randomly divided into five groups (eight mice per group) (day 0). On the same day, the five groups were treated with saline (NS), Blank NPs, Sal free 2 (2 mg/kg, once every 2 days for four times), Sal NP 8 (8 mg/kg, once), or Sal NP 2 (2 mg/kg, once every 2 days for four times). Tumor size was measured once every 2 days during the study. The tumor volume was calculated using the formula: $W^2 \times L/2$, where W is the widest diameter, and L is the longest diameter. Relative tumor volumes were calculated using the following equation to reduce the

impact of initial tumor volume differences after grouping: Relative tumor volume=V/V0, where *V* was the absolute tumor volume and *V0* was the average tumor volume of the group on day 0. On day 14, the mice were sacrificed, and tumors were collected for pathological study by hematoxylin and eosin (H&E) staining.

Systemic Toxicity

Tumor pieces (3 × 3 × 3 mm) were subcutaneously implanted on the right axilla of male BALB/c nude mice (age: 4–5 weeks, weight: 18–22 g), housed under SPF conditions. The mice whose tumor volumes reached approximately 100–200 mm^3 were randomly divided into five groups (eight mice per group) (day 0). On the same day, the mice were treated with NS, Blank NPs, Sal NP 2 (2 mg/kg, once every 2 days for four times), Sal free 2 (2 mg/kg, once every 2 days for four times), and Sal NP 8 (8 mg/kg, once). Survival was observed during the treatment period for approximately 14 days. The weights of the mice were also measured once every 2 days. Their activity and appetite were also observed. On day 14, the mice were sacrificed. Hearts, lungs, livers, spleens, and kidneys were collected for H&E staining to assess the systemic toxicity in each group.

Immunohistochemistry (IHC)

The tumor tissues from the mice that received NS, Blank NP, Sal free 2, Sal NP 2, and Sal NP 8 were used for IHC. Sections (4-mm thick) from paraffin-embedded tumors were deparaffinized and rehydrated using xylene and ethanol, respectively, and immersed in 3% hydrogen peroxide solution for 10 min to block endogenous peroxidases. Sections were boiled for 30 min in 10 mM citrate buffer solution (pH 6.0) for antigen retrieval. Slides were incubated for 45 min with 5% bovine serum albumin and incubated overnight at 4°C with anti-proliferating cell nuclear antigen (anti-PCNA) (Abcam, USA), anti-Ki-67 (Abcam, USA), anti-Caspase3 (Abcam, USA), anti-CD44, anti-CD133, anti-E-cadherin, and anti–VIM antibodies. These specimens were incubated for 45 min at 37°C with the appropriate peroxidase-conjugated secondary antibody (Abcam, USA) and visualized using the Real Envision Detection Kit (Gene Tech Shanghai Company Limited, Shanghai, China) following the instructions provided by the manufacturer. All slides were counter-stained with H&E.

WB Assays

The tumor tissues obtained from the mice that received treatment with NS, Blank NP, Sal free 2, Sal NP 2, and Sal NP 8 were selected for further study. These tissues were ground into cell suspensions. Cells were washed twice with phosphate-buffered saline (PBS) solution and lysed with RIPA Lysis Buffer (Beyotime Institute of Biotechnology, Shanghai, China) and protease inhibitor (Thermo Fisher Scientific, USA). Protein concentrations were determined using the Pierce BCA Protein Assay Kit (Thermo Fisher Scientific, USA). Equivalent amounts of total protein (60 μg) were boiled and electrophoretically separated on a 10% polyacrylamide gel at 80 volts. The proteins were transferred onto polyvinylidene difluoride membranes. The membranes were blocked for 60 min with a 5% milk solution prepared in PBS, incubated overnight at 4°C with primary antibodies (GAPDH, CD44, CD133, E-cadherin, VIM, ZEB1, and ZEB2) at a 1:500 dilution. The membranes were washed thrice for 5 min each time with Tween 20 (1:1000 dilution)-PBS and incubated for 45 min with the appropriate peroxidase-conjugated secondary antibody (Abcam, USA) (1:1000 dilution). Membranes were washed with Tween 20-PBS thrice for 10 min each time and visualized using the Odyssey two-color infrared laser imaging system (ECDOI, Greenville, USA). The signal generated by GAPDH was used as an internal control.

Flow Cytometric Analysis of Tumor-Derived Cells

The expression of the CD44 marker on cells obtained from HeLa tumors of xenografts models was distinctly evaluated using flow cytometric analysis. Cell staining was performed on tumors excised from each mouse of the five treatment groups (i.e., NS, Blank NP, Sal NP 2, Sal free 2, and Sal NP 8) after four repeated treatments. Prior to digestion with collagenase, xenograft tumors were cut into small pieces. The tumor pieces were subsequently mixed with collagenase III and incubated at 37°C for 15–20 min for enzymatic dissociation to obtain single-cell suspensions. At the end of the incubation, cells were filtered through a 40-mm cell strainer and washed with RPMI-1640 with 20% fetal bovine serum and PBS. Subsequently, the cells were immunostained with anti-CD44-PE (BD, New Jersey, USA) at 4°C for 20 min. The samples were washed and resuspended in 500 μL of cold PBS, and analyzed through flow cytometry (BD FACS Aria II, BD Biosciences, San Jose, CA, USA).

Tumor Seeding Study

Tumor tissues obtained from the mice that received treatment with NS and Sal NP 2 were selected for further study. We cut the tumor tissues into pieces (3 × 3 × 3 mm) and placed them into a petri dish containing saline. The mice were randomly divided into four groups (five mice per group) and anesthetized. Tumor pieces were subcutaneously implanted on the right axilla of the mice. Subsequently, we measured the rates of tumor formation and growth.

Statistical Analysis

The Student's *t*-test (two tailed) was used for statistical analyses. P-values <0.05 denoted statistically significant differences.

Results

Real-Time Biodistribution of NPs After Systematic Administration in Tumor-Bearing Mice

We marked the Sal NPs with a NIRF dye (NIR-797) for NIRF imaging, to visualize the real-time biodistribution of Sal NPs in xenograft tumor-bearing mice. The NIR fluorescence signals were observed on tumors and the abdomen 24-h post IP injection (Figure 1 and Supplemental Figure 1). The fluorescence density of the abdomen decreased with time, whereas NIRF signals gradually increased in the tumor. Following 48 h post administration, the strong fluorescence signal was mostly observed in the tumor region, indicating that the systematic IP administration of Sal NPs can intelligently target the tumor region.

In vivo Anticancer Efficacy of Sal NPs

The antitumor efficacy of Sal NPs was evaluated using a subcutaneous HeLa tumor-bearing BALB/c nude mice model. The experimental groups included NS, Blank NPs, Sal free 2 (2 mg/kg, once every 2 days for four times), Sal NP 2 (2 mg/kg, once every 2 days for four times), and Sal NP 8 (8 mg/kg, once). We did not include a "Sal free 8" group because, according to our previous findings,[41] this dose of free Sal was lethal to mice. On day 12 after the first treatment, the tumor inhibition rates in the Sal free 2, Sal NP 2, and Sal NP 8 groups were 48.2%, 65.7%, and 64.3%, respectively (Figure 2A). The Sal NP 2-treated group showed higher antitumor efficiency and smaller tumor volumes (P<0.001 of 8 mg/kg Sal free 2 equal) than the Sal free 2-treated group. Compared with Sal free 2, Sal NPs began to show its antitumor efficacy after the first 6 days. The antitumor advantages of Sal NPs became more prominent with time (P<0.001). Sal NP 8 exerted a similar antitumor effect to that of Sal NP 2, indicating the sustainable release and effectiveness of NPs.

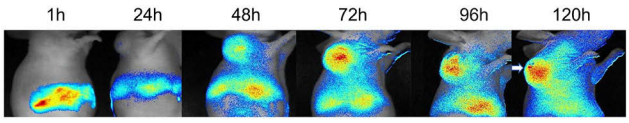

Figure 1 INIRF images. HeLa tumor bearing mice were systematically injected of NIR-797 labeled Sal NPs, and observed for a period of 120h. The tumors were marked by arrows. The images of 7 time points were showed to analysis the acumination of Sal NPs in tumor region and normal organs. In the NIRF images, NPs administrated by systematically administration could accumulate into tumor region, which showed the intelligent targeting ability of our NPs.
Abbreviations: NIRF, near-infrared fluorescence; Sal NPs, Sal-mPEG-pep-PCL nanoparticles; NPs, nanoparticles.

Furthermore, pathological studies of the tumors were conducted as supplements of the tumor size study (Figure 2B). Crowded tumor cells with large and hyperchromatic nuclei were observed in the control group and Blank NP group, while necrotic regions were rare. In the Sal free 2 treatment group, sporadic small areas of pink staining and karyopyknosis were observed in some tumor cells. In the Sal NP 8 group, the discrete necrotic regions were more obvious and exhibited cell apoptosis. The phenomenon became most prominent in the Sal NP 2 groups, explaining the smallest tumor volumes at the pathological level. We next studied the cell growth activity using PCNA, Ki-67, and Caspase3 staining. As shown in Figure 2C, treatment with Sal induced tumor apoptosis and inhibited tumor proliferation. This was evidenced by a significant increase in the expression of Caspase3 and decrease in that of Ki-67 and PCNA. Compared with the Sal free-treated group, the Sal NP-treated groups showed a greater inhibitory effect on cancer cells, confirming the target capacity and sustainable release of NPs.

In vivo Toxicity Study

H&E-stained sections of important organs (Figure 3A) and body weight variations (Figure 3B) were examined to evaluate the adverse effects of Sal NPs and Sal free. The number of surviving mice was counted to preliminarily evaluate the safety of Sal NPs in vivo. All BALB/c nude mice survived after IP injection of Sal NPs at an equivalent Sal dose of 8 mg/kg, a dose that exceeded the lethal dose of Sal (Table 1). Compared with the Sal free 2-treated group, mice in the Sal NP 2- and Sal NP 8-treated groups did not show changes in their body weight (P<0.001). Moreover, there was no obvious change in H&E staining of the lung, liver, heart, kidney, spleen, and skeletal

muscle (Figure 3B), indicating the in vivo safety of Sal NPs. However, in the Sal free 2-treated group, an obvious change in H&E staining of the lung was observed. Specifically, alveolar interstitial hyperemia, edema, and inflammatory cell infiltration were observed in lung tissues, which may lead to respiratory failure or even death. Moreover, the liver showed a vascular glass-like change and inflammatory cell infiltration. The heart muscle also exhibited inflammatory cell infiltration. The hematopoietic spleen had obvious histocyte aggregation, indicating the presence of significant inflammation (Supplemental Figure 2). Thus, the Sal NPs can reduce the side effects of Sal.

Sal Inhibits the Stem-Like Properties of HeLa Cells in vivo

We next examined the expression of the cervical CSC-related markers CD44 and CD133.[42,43] The IHC and WB analyses showed that mice receiving Sal exhibited markedly lower levels of CD133 and CD44 than their control counterparts (Figure 4A and C). Among all the groups, the Sal NP 2-treated group showed the strongest inhibition of CSCs. We also evaluated the expression of CD44, a main marker used for the identification of CSCs in CC, to further determine whether the CSC phenotype of cells could be affected by Sal NPs.[44] According to the cytometric analysis, in the

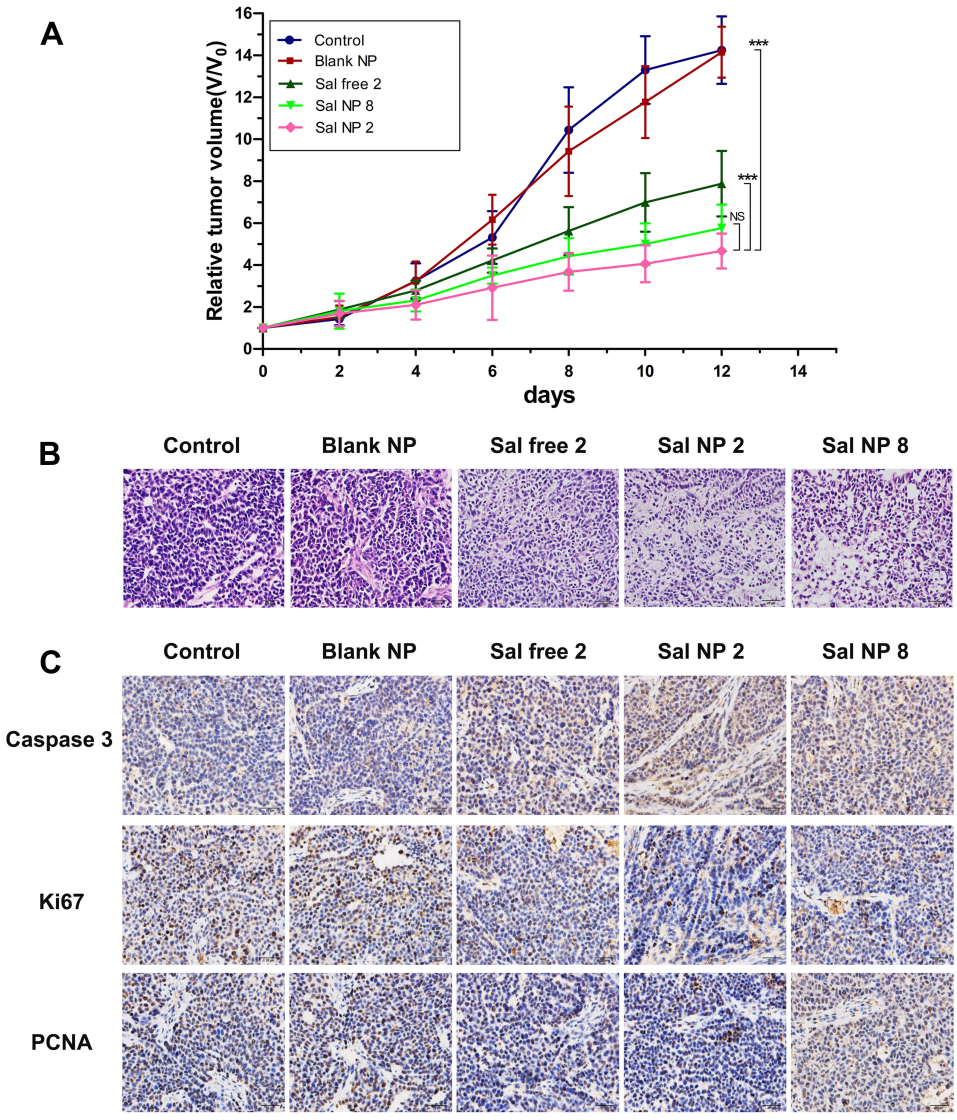

Figure 2 In vivo antitumor efficacy of Sal and Sal NPs in a HeLa tumor model. (**A**) The tumor growth curves of HeLa tumor-bearing mice that received different treatments (n=8) ***p<0.001; (**B**) H&E staining of the tumors in different treatment groups (n=8); (**C**) Representative IHC staining of Ki-67, Caspase3 and PCNA of the cervical tumors in day 12.

Abbreviations: Sal, Salinomycin; Sal NPs, Sal-mPEG-pep-PCL nanoparticles; H&E, hematoxylin and eosin; IHC, Immunohistochemistry.

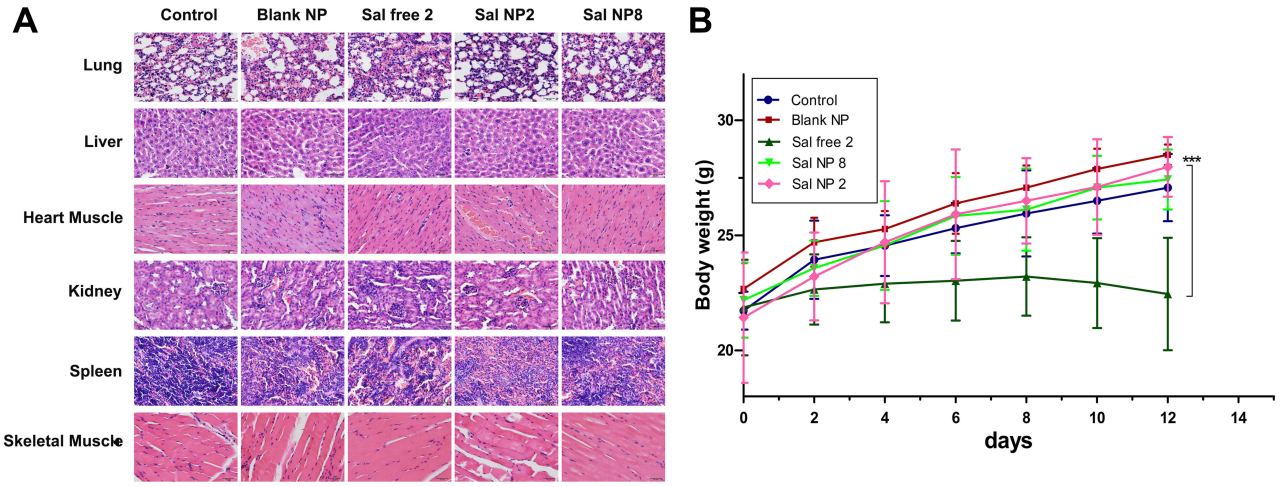

Figure 3 In vivo toxicity analysis of Sal and Sal NPs. (**A**): Histological analyses of organ toxicity through H&E staining (×200) after treatment with control, Blank NP, Sal free 2, Sal NP 2, Sal NP 8; (**B**): Weight loss profiles over time after various treatments (n=8) ***p<0.001.
Abbreviations: Sal, Salinomycin; Sal NPs, Sal-PEG-pep-PCL nanoparticles; H&E, hematoxylin and eosin; Sal free 2, salinomycin solvent 2 mg/kg, every other day for four times; Sal NP 2, Sal NPs 2mg/Kg, every other day for 4 times; Sal NP 8, Sal NPs 8mg/kg, once.

untreated group, HeLa cancer cells highly expressed CD44 (mean: 21.9%). Treatment with Sal NP 2 significantly decreased the expression of CD44 (mean: 6.55%), while Sal free 2 also decreased the percentage of CD44-positive HeLa cells to 13.8% (Figure 4B). However, the mechanism involved in this process remains unknown, and further study is warranted.

Sal NPs Inhibited the EMT Pathway of HeLa Cells in vivo

The IHC and WB analyses of E-cadherin and VIM showed an increased expression of the former and reduced expression of the latter, highlighting the inhibitory property of Sal on the EMT process (Figure 5A and B). It has been reported that EMT is regulated by several transcription factors, including ZEB1and ZEB2, which inhibit the epithelial phenotype and repress E-cadherin transcription.[45–47] The WB analysis revealed that the expression of ZEB1 and ZEB2 decreased after treatment with Sal (Figure 5C and Supplemental Table 1). Meanwhile, among the Sal-treated groups, the Sal NP 2 group showed lower expression of VIM, ZEB1, and ZEB2 and higher expression of E-cadherin than the Sal free 2 group. However, it did not show a significant difference with the Sal NP 8 treatment group.

Sal Suppresses the Tumor Regenerative Ability of HeLa Cells

We implanted fresh CC specimens obtained from two treatment groups (ie, NS and Sal NP 2) in nude mice to further demonstrate the biological effectiveness of Sal NPs on CCSCs and EMT characteristics of tumor cells from CC tissues after anticancer treatment. Subsequently, we investigated the tumorigenic capacity and growth speed of these tumor-bearing mice under the same conditions.

Table 1 Survival of Mice After Sal Treatment in Solution and NPs Formation

Group	Number of Live Mice							
	Day 0	Day 2	Day 4	Day 6	Day 8	Day 10	Day 12	Day 14
A	8	8	8	8	8	8	8	8
B	8	8	8	8	8	8	8	8
C	8	8	8	6	5	4	3	2
D	8	8	8	8	8	8	8	8
E	8	8	8	8	8	8	8	8

Notes: A: Control; B: Blank NP; C: Sal free 2; D: Sal NP 2; E: Sal NP 8; Sal free 2 (2 mg/kg, every other day for 4 times); Sal NP 8 (8mg/Kg, once); Sal NP 2 (2mg/Kg, every other day for 4 times).

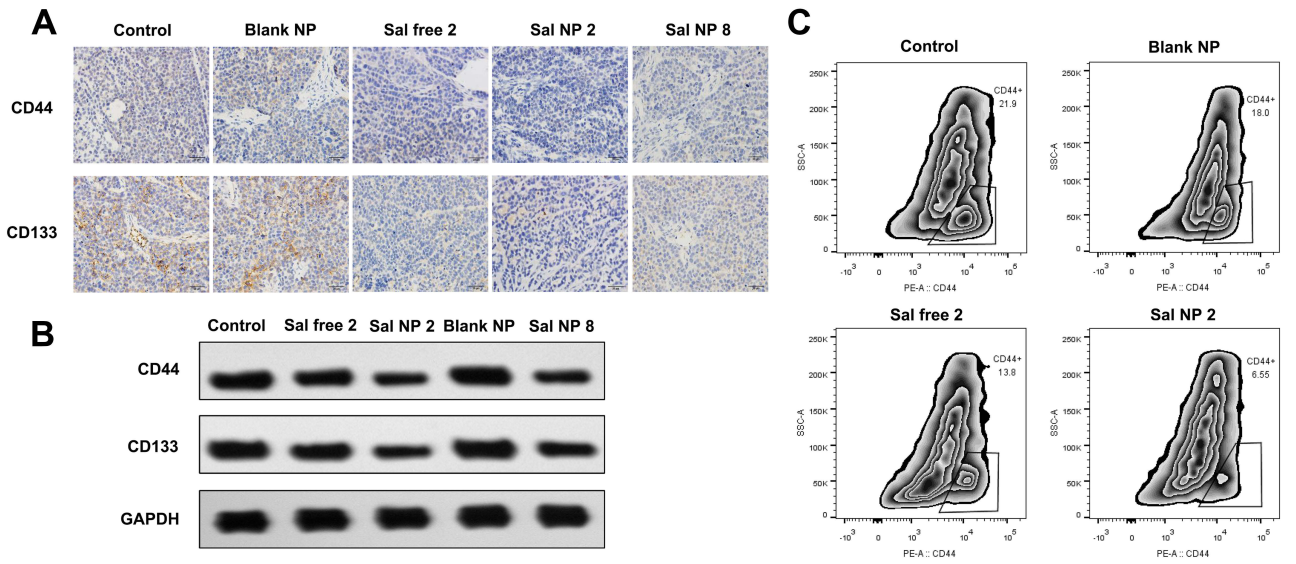

Figure 4 Sal NPs inhibits stem like properties of CC in vivo. The IHC (**A**) and WB (**B**) and analysis of CD44 and CD133 variation in tumors of various treatment groups. Sal NP 2 groups showed the decreased expression of CD44 and CD133 than control group, which demonstrated the CCSCs inhibition capacity of Sal NPs; Flow cytometric analysis (**C**) indicated the strongest inhibition ability of Sal NP on cancer stem cells.

Abbreviations: Sal NPs, Sal-PEG-pep-PCL nanoparticles; CC, cervical cancer; IHC, Immunohistochemistry; WB, Western blot analysis; Sal NP 2, Sal NPs 2mg/Kg, every other day for 4 times; CCSC, cervical cancer stem cells.

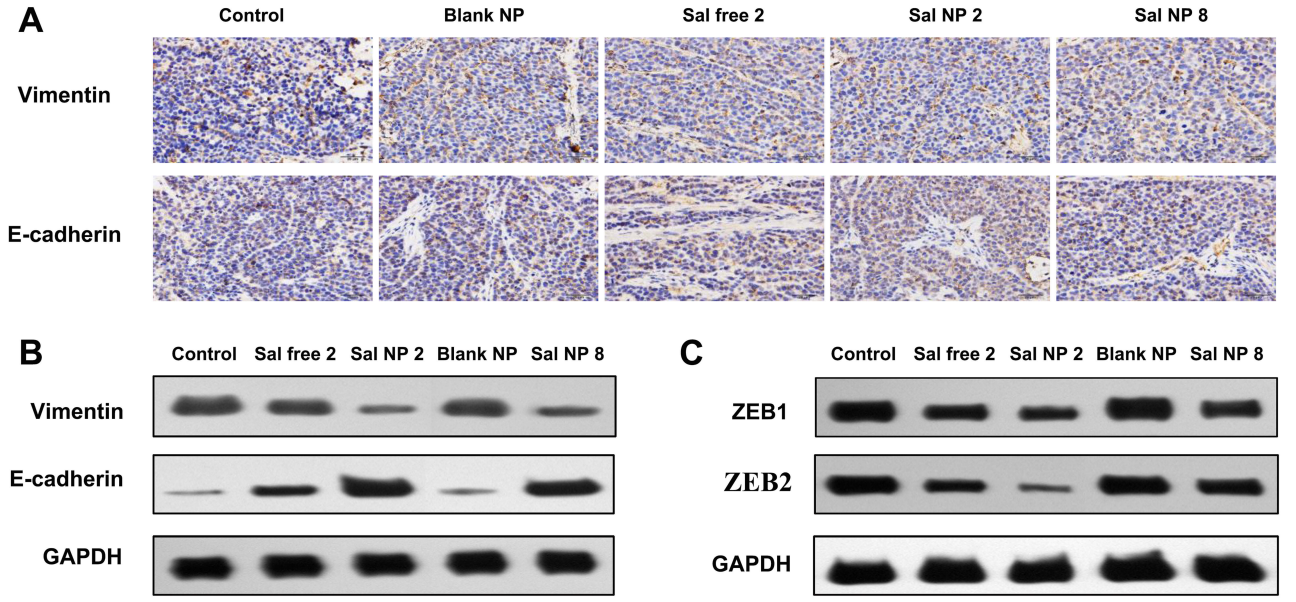

Figure 5 Mechanism of CCSCs inhibition by Sal NPs. IHC (**A**) and WB (**B**) result of E-cadherin, VIM proteins expression changes after different antitumor treatments; Both Sal free and Sal NPs groups showed the lower expression of VIM and higher expression of E-cadherin than control group and Sal NP 2 showed the lowest expression among all treatment groups; WB analysis (**C**) of EMT transcription regulators demonstrated that Sal can inhibit EMT pathway.

Abbreviations: CCSC, cervical cancer stem cells; Sal NPs, Sal-PEG-pep-PCL nanoparticles; IHC, Immunohistochemistry; WB, Western blot analysis; Sal NP 2, Sal NPs 2mg/Kg, every other day for 4 times; Sal free 2, salinomycin solvent 2 mg/kg, every other day for four times; EMT, Epithelial interstitial transformation.

Figure 6B shows that tumor spheres could be observed in 100% (5/5) of the mice in the NS group 9 days after implantation, while 40% (2/5) of the mice in the Sal NP 2 group showed tumor formation. During the observation period, one mouse in the Sal NP 2 group did not regenerate its tumor. As shown in Figure 6A, Sal NP 2 delayed tumor growth compared with the NS groups ($P<0.001$). These findings indicated that treatment with Sal NP 2

A

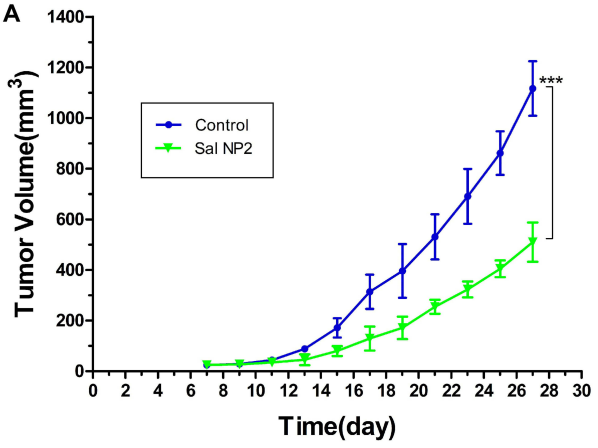

B

Tumorigenic capacity of secondary tumors

Group	Time				
	Day7	Day9	Day11	Day13	Day15
Control	4/5	5/5	5/5	5/5	5/5
Sal NP2	2/5	2/5	3/5	4/5	4/5

Sal NP2 (2mg/Kg, every other day for 4 times)

Figure 6 Tumor reseeding assay and growth curves of secondary tumors. Freshly gastric cancer specimens of two treatment groups (Control and Sal NP 2) were transplanted into another nude mice. The tumor regeneration ability (**B**) and the growth speed (**A**) of these tumor-bearing mice under the same conditions were investigated, ***p<0.001.

Abbreviation: Sal NP 2, Sal NPs 2mg/Kg, every other day for 4 times.

decreased the seeding ability and growth speed of tumor cells.

Discussion and Conclusion

As a drug delivery system, NPs have drawn increasing attention owing to their unique characteristics.[48–50] The solubility of Sal can be improved by incorporation into the core of NPs.[51,52] Therefore, NPs may be a suitable drug delivery system for Sal. In our previous research, we designed intelligent gelatinase-stimuli NPs for the targeted delivery of Sal. These NPs are modified by inserting the optimal gelatinase-cleavable peptide (PVGLIG) between the mPEG and PCL segments (mPEG-peptide-PCL).[53] Owing to their special structures, the NPs prepared from mPEG-peptide-PCL exhibit their own characteristics, such as prolonged circulation time and accumulation in the tumor site by the EPR effect.[54–56] MMPs are abundantly present in tumors,[57,58] and have been considered as tumor-specific stimuli for cancer imaging and drug delivery.[59,60] Following the accumulation of NPs in the tumors, the mPEG-peptide-PCL conjugates will be cleaved at a certain site of the MMP2/9 peptide by MMP2/9. The dePEGylated NPs can be retained in the tumor regions, which can effectively interact with additional tumor cells. In addition, the cellular uptake can be increased to improve the intracellular concentration of anticancer drugs. Furthermore, the expression of MMPs is similar to that of CSC-related markers and single pathways, such as the EMT pathway.[61,62] Moreover, EMT promotes tumor cell aggressiveness by increasing the expression of MMPs, especially gelatinases.[63] Thus, we hypothesized that Sal NPs can target cancer cells and CSCs through a gelatinase-stimuli strategy. Previous studies have reported that our gelatinase-stimuli NPs showed superior performance as a delivery system for docetaxel or 5-fluorouracil.[64,65] They can be used to improve solubility, increase accumulation in the tumor, and decrease the occurrence of side effects.[66,67] Therefore, we used these gelatinase-stimuli NPs for the delivery of Sal to improve its solubility, which further contributes to increased drug enrichment in tumors and enhanced inhibitory capacity of CSCs. Of note, the adverse effects were significantly milder than those reported in the Sal free-treated group.

According to our previous study, the hydrophobic Sal can be encapsulated into NPs to generate a soluble form which can be stably dispersed in water.[68–70] Encapsulating Sal into NPs significantly reduced its side effects, since there were no obvious pathological changes observed in the H&E staining of important organs, body weight variations, and survival. NIRF imaging also revealed the prolonged accumulation of Sal NPs in tumor sites after systematic administration. Thus, Sal may sustainably target tumor regions, and exhibits a good tolerability profile in vivo with low toxicity.

An in vivo anti-tumor study demonstrated that Sal NPs effectively suppressed tumor growth with lower proliferation and higher apoptosis levels than those recorded in other groups.[71] Anti-tumor agents mainly exert anti-tumor effects through induction of apoptosis. Caspase function, which serves as the central regulator in cell death, is activated upon cell apoptosis.[72] Ki-67 and PCNA are commonly used markers of cell proliferation.[73] Their high expression indicates a greater potential for tumors to present the metastatic phenotype. In this study, Sal induced apoptosis and inhibited the proliferation CC cells in vivo, as evidenced by the upregulation of pro-apoptotic factor Caspase3 and down-regulation of Ki-67 and PCNA in tumor specimens.

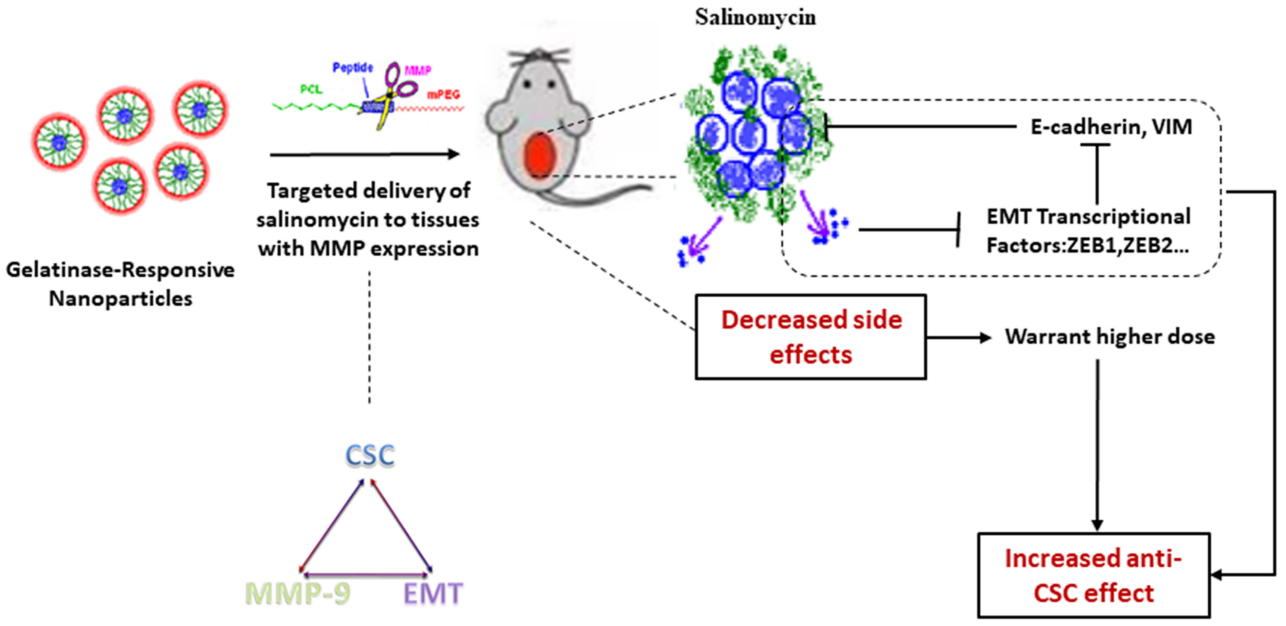

Scheme 1 Schematic illustration of targeting CCSC by incorporating Sal into gelatinases-stimuli NPs. CCSC were inhibited by down regulating EMT signaling pathway.
Abbreviations: CCSC, cervical cancer stem cells; Sal, salinomycin; NPs, nanoparticles; EMT, Epithelial interstitial transformation.

Our data demonstrated that Sal NP 2 and Sal free 2 decreased the expression of CD44 and CD133 in CC tissues and the tumor seeding ability. The flow cytometric analysis also directly presented the decreased proportion of CD44-positive CSCs. In the tumor reseeding study, the Sal NP 2 group showed the slowest tumor growth pattern in comparison with the other groups, demonstrating the predominant inhibitory effect of Sal on CSC.

EMT is closely associated with CSCs, and promotes tumor invasion and metastasis.[74–76] The loss of E-cadherin is a hallmark for EMT;[77] thus, we investigated the expression of E-cadherin and VIM. In the Sal NPs-treated groups, the expression of E-cadherin increased, whereas that of VIM decreased. These findings supported the fact that Sal can specifically inhibit CSC by attenuating the EMT pathway. ZEB1 and ZEB2 are negative inducers of EMT,[78,79] which enable tumor cells to invade and metastasize to distant sites. We examined changes in the expression of EMT-related genes (i.e., E-cadherin and VIM) using qualitive IHC and quantitative WB to gain insight into the impact of Sal effects on the stemness of HeLa CC cells. Furthermore, the levels of ZEB1 and ZEB2 proteins were markedly reduced after treatment with Sal. These results indicated that Sal inhibited CSCs by targeting ZEB1 and ZEB2 to regulate the EMT process in CC.

As illustrated in Scheme 1, an anti-CSC drug delivery system (Sal-PEG-peptide-PCL NPs) was prepared. The Sal NPs significantly decreased the proportion of CSCs, tumorigenic capacity, and growth speed in tumor-bearing mice. It is noteworthy that the side effects of Sal could be relieved through encapsulation into NPs, which facilitates the application of Sal to humans. However, the mechanism involved in the inhibition of CSCs by Sal is obscure, underlining the need for further research prior to any application in clinical practice.

Acknowledgments

This work has been supported by the National Natural Science Foundation of China (grant numbers 81672398, 81972192, and 81930080), the 5th group of "333 talent project" of Jiangsu Province (grant number Ⅲ-0119, 2016), the 14th group of six talent peak project in Jiangsu province (grant number YY-068), and the Medical youth talent project of Jiangsu Province (grant number QNRC2016044).

Author Contributions

Qin Wang and Fangcen Liu contributed equally to this work. Baorui Liu and Rutian Li are both corresponding authors of this work. All authors contributed to data analysis, drafting and revising the article, gave final approval of the version to be published, and agree to be accountable for all aspects of the work.

Disclosure

The authors confirm they have no known conflicts of interest associated with this publication.

References

1. Kamangar F, Dores GM, Anderson WF. Patterns of cancer incidence, mortality, and prevalence across five continents: defining priorities to reduce cancer disparities in different geographic regions of the world. *J Clin Oncol*. 2006;24(14):2137–2150. doi:10.1200/JCO.2005.05.2308
2. Ademuyiwa FO, Bshara W, Attwood K. NY-ESO-1 cancer testis antigen demonstrates high immunogenicity in triple negative breast cancer. *PLoS One*. 2012;7(6):e38783. doi:10.1371/journal.pone.0038783
3. Bray F, Ferlay J, Soerjomataram I, Siegel RL, Torre LA, Jemal A. Global cancer statistics 2018: GLOBOCAN estimates of incidence and mortality worldwide for 36 cancers in 185 countries. *CA Cancer J Clin*. 2018;68:394–424.
4. Liu B, Han L, Liu J, Han S, Chen Z, Jiang L. Co-delivery of paclitaxel and TOS-cisplatin via TAT-targeted solid lipid nanoparticles with synergistic antitumor activity against cervical cancer. *Int J Nanomedicine*. 2017;12:955–968. doi:10.2147/IJN
5. Wang AH, Zhao JM, Du J, Pang QX, Wang MQ. Long noncoding RNA LUCAT1 promotes cervical cancer cell proliferation and invasion by upregulating MTA1. *Eur Rev Med Pharmacol Sci*. 2019;23(16):6824–6829. doi:10.26355/eurrev_201908_18721
6. Kumar L, Harish P, Malik PS, Khurana S. Chemotherapy and targeted therapy in the management of cervical cancer. *Curr Probl Cancer*. 2018;42(2):120–128. doi:10.1016/j.currproblcancer.2018.01.016
7. Dong W, Chen A, Chao X, et al. Chrysin inhibits proinflammatory factor-induced EMT phenotype and cancer stem cell-like features in HeLa Cells by blocking the NF-kappaB/Twist axis. *Cell Physiol Biochem*. 2019;52(5):1236–1250.
8. Huang R, Rofstad EK. Cancer stem cells (CSCs), cervical CSCs and targeted therapies. *Oncotarget*. 2017;8(21):35351–35367. doi:10.18632/oncotarget.10169
9. Santin AD, Sill MW, McMeekin DS, et al. Phase II trial of cetuximab in the treatment of persistent or recurrent squamous or non-squamous cell carcinoma of the cervix: a Gynecologic Oncology Group study. *Gynecol Oncol*. 2011;122(3):495–500.
10. Menderes G, Black J, Schwab CL, Santin AD. Immunotherapy and targeted therapy for cervical cancer: an update. *Expert Rev Anticancer Ther*. 2016;16(1):83–98. doi:10.1586/14737140.2016.1121108
11. Gyawali B, Iddawela M. Bevacizumab in advanced cervical cancer: issues and challenges for low- and middle-income countries. *J Global Oncol*. 2017;3(2):93–97. doi:10.1200/JGO.2016.004895
12. Cohen PA, Jhingran A, Oaknin A, Denny L. Cervical cancer. *Lancet*. 2019;393(10167):169–182. doi:10.1016/S0140-6736(18)32470-X
13. Wang L, Liu Y, Zhou Y, et al. Zoledronic acid inhibits the growth of cancer stem cell derived from cervical cancer cell by attenuating their stemness phenotype and inducing apoptosis and cell cycle arrest through the Erk1/2 and Akt pathways. *J Exp Clin Cancer Res*. 2019;38(1):93. doi:10.1186/s13046-019-1109-z
14. Lopez J, Poitevin A, Mendoza-Martinez V, Perez-Plasencia C, Garcia-Carranca A. Cancer-initiating cells derived from established cervical cell lines exhibit stem-cell markers and increased radioresistance. *BMC Cancer*. 2012;12:48. doi:10.1186/1471-2407-12-48
15. Baccelli I, Trumpp A. The evolving concept of cancer and metastasis stem cells. *J Cell Biol*. 2012;198(3):281–293. doi:10.1083/jcb.201202014
16. Wang K, Zeng J, Luo L, et al. Identification of a cancer stem cell-like side population in the HeLa human cervical carcinoma cell line. *Oncol Lett*. 2013;6(6):1673–1680. doi:10.3892/ol.2013.1607
17. Ding Y, Yu AQ, Li CL, Fang J, Zeng Y, Li DS. TALEN-mediated *Nanog* disruption results in less invasiveness, more chemosensitivity and reversal of EMT in Hela cells. *Oncotarget*. 2014;5(18):8393–8401. doi:10.18632/oncotarget.v5i18
18. Cooke SL, Temple J, Macarthur S, et al. Intra-tumour genetic heterogeneity and poor chemoradiotherapy response in cervical cancer. *Br J Cancer*. 2011;104(2):361–368. doi:10.1038/sj.bjc.6605971
19. Mendoza-Almanza G, Ortiz-Sanchez E, Rocha-Zavaleta L, Rivas-Santiago C, Esparza-Ibarra E, Olmos J. Cervical cancer stem cells and other leading factors associated with cervical cancer development. *Oncol Lett*. 2019;18(4):3423–3432. doi:10.3892/ol.2019.10718
20. Gupta PB, Onder TT, Jiang G, et al. Identification of selective inhibitors of cancer stem cells by high-throughput screening. *Cell*. 2009;138(4):645–659.
21. Zhou J, Li P, Xue X, et al. Salinomycin induces apoptosis in cisplatin-resistant colorectal cancer cells by accumulation of reactive oxygen species. *Toxicol Lett*. 2013;222(2):139–145. doi:10.1016/j.toxlet.2013.07.022
22. Zhang GN, Liang Y, Zhou LJ, et al. Combination of salinomycin and gemcitabine eliminates pancreatic cancer cells. *Cancer Lett*. 2011;313(2):137–144. doi:10.1016/j.canlet.2011.05.030
23. Klose J, Guerlevik E, Trostel T, et al. Salinomycin inhibits cholangiocarcinoma growth by inhibition of autophagic flux. *Oncotarget*. 2018;9(3):3619–3630. doi:10.18632/oncotarget.v9i3
24. Liu L, Wang Q, Mao J, et al. Salinomycin suppresses cancer cell stemness and attenuates TGF-beta-induced epithelial-mesenchymal transition of renal cell carcinoma cells. *Chem Biol Interact*. 2018;296:145–153. doi:10.1016/j.cbi.2018.09.018
25. Yue W, Hamai A, Tonelli G, et al. Inhibition of the autophagic flux by salinomycin in breast cancer stem-like/progenitor cells interferes with their maintenance. *Autophagy*. 2013;9(5):714–729. doi:10.4161/auto.23997
26. Mai TT, Hamai A, Hienzsch A, et al. Salinomycin kills cancer stem cells by sequestering iron in lysosomes. *Nat Chem*. 2017;9(10):1025–1033. doi:10.1038/nchem.2778
27. Huang X, Borgstrom B, Stegmayr J, et al. The molecular basis for inhibition of stemlike cancer cells by salinomycin. *ACS Central Sci*. 2018;4(6):760–767. doi:10.1021/acscentsci.8b00257
28. Dorne JL, Fernandez-Cruz ML, Bertelsen U, et al. Risk assessment of coccidostatics during feed cross-contamination: animal and human health aspects. *Toxicol Appl Pharmacol*. 2013;270(3):196–208. doi:10.1016/j.taap.2010.12.014
29. Boehmerle W, Muenzfeld H, Springer A, Huehnchen P, Endres M. Specific targeting of neurotoxic side effects and pharmacological profile of the novel cancer stem cell drug salinomycin in mice. *J Mol Med*. 2014;92(8):889–900. doi:10.1007/s00109-014-1155-0
30. Story P, Doube A. A case of human poisoning by salinomycin, an agricultural antibiotic. *N Z Med J*. 2004;117(1190):U799.
31. Zhang Y, Zhang H, Wang X, Wang J, Zhang X, Zhang Q. The eradication of breast cancer and cancer stem cells using octreotide modified paclitaxel active targeting micelles and salinomycin passive targeting micelles. *Biomaterials*. 2012;33(2):679–691. doi:10.1016/j.biomaterials.2011.09.072
32. Zhang ZT, Huang-Fu MY, Xu WH, Han M. Stimulus-responsive nanoscale delivery systems triggered by the enzymes in the tumor microenvironment. *Eur J Pharm Biopharm*. 2019;137:122–130. doi:10.1016/j.ejpb.2019.02.009
33. Mo L, Zhao Z, Hu X, et al. Smart nanodrug with nuclear localization sequences in the presence of MMP-2 to overcome biobarriers and drug resistance. *Chemistry*. 2019;25(8):1895–1900. doi:10.1002/chem.v25.8
34. Blanco E, Shen H, Ferrari M. Principles of nanoparticle design for overcoming biological barriers to drug delivery. *Nat Biotechnol*. 2015;33(9):941–951. doi:10.1038/nbt.3330

35. Wang S, Huang P, Chen X. Stimuli-responsive programmed specific targeting in nanomedicine. *ACS Nano*. 2016;10(3):2991–2994. doi:10.1021/acsnano.6b00870
36. Yadav L, Puri N, Rastogi V, Satpute P, Ahmad R, Kaur G. Matrix metalloproteinases and cancer - roles in threat and therapy. *Asian Pac J Cancer Prev*. 2014;15(3):1085–1091. doi:10.7314/APJCP.2014.15.3.1085
37. Alaseem A, Alhazzani K, Dondapati P, Alobid S, Bishayee A, Rathinavelu A. Matrix Metalloproteinases: A challenging paradigm of cancer management. *Semin Cancer Biol*. 2017;56:100–115.
38. Kessenbrock K, Plaks V, Werb Z. Matrix metalloproteinases: regulators of the tumor microenvironment. *Cell*. 2010;141(1):52–67. doi:10.1016/j.cell.2010.03.015
39. Jia S, Qu T, Wang X, et al. KIAA1199 promotes migration and invasion by Wnt/beta-catenin pathway and MMPs mediated EMT progression and serves as a poor prognosis marker in gastric cancer. *PLoS One*. 2017;12(4):e0175058. doi:10.1371/journal.pone.0175058
40. Mao W, Sun Y, Zhang H, Cao L, Wang J, He P. A combined modality of carboplatin and photodynamic therapy suppresses epithelial-mesenchymal transition and matrix metalloproteinase-2 (MMP-2)/MMP-9 expression in HEp-2 human laryngeal cancer cells via ROS-mediated inhibition of MEK/ERK signalling pathway. *Lasers Med Sci*. 2016;31(8):1697–1705. doi:10.1007/s10103-016-2040-6
41. Wang Q, Wu P, Ren W, et al. Comparative studies of salinomycin-loaded nanoparticles prepared by nanoprecipitation and single emulsion method. *Nanoscale Res Lett*. 2014;9(1):351. doi:10.1186/1556-276X-9-351
42. Organista-Nava J, Gomez-Gomez Y, Garibay-Cerdenares OL, Leyva-Vazquez MA, Illades-Aguiar B. Cervical cancer stem cell-associated genes: prognostic implications in cervical cancer. *Oncol Lett*. 2019;18(1):7–14. doi:10.3892/ol.2019.10307
43. Ortiz-Sanchez E, Santiago-Lopez L, Cruz-Dominguez VB, et al. Characterization of cervical cancer stem cell-like cells: phenotyping, stemness, and human papilloma virus co-receptor expression. *Oncotarget*. 2016;7(22):31943–31954. doi:10.18632/oncotarget.v7i22
44. Takaishi S, Okumura T, Tu S, et al. Identification of gastric cancer stem cells using the cell surface marker CD44. *Stem Cells*. 2009;27(5):1006–1020. doi:10.1002/stem.v27:5
45. Zhang H, Zhang Y, Chen C, et al. A double-negative feedback loop between DEAD-box protein DDX21 and Snail regulates epithelial-mesenchymal transition and metastasis in breast cancer. *Cancer Lett*. 2018;437:67–78. doi:10.1016/j.canlet.2018.08.021
46. Zhang Z, Xu J, Liu B, et al. Ponicidin inhibits pro-inflammatory cytokine TNF-alpha-induced epithelial-mesenchymal transition and metastasis of colorectal cancer cells via suppressing the AKT/GSK-3beta/Snail pathway. *Inflammopharmacology*. 2018;27:627–638.
47. Zheng M, Jiang YP, Chen W, et al. Snail and Slug collaborate on EMT and tumor metastasis through miR-101-mediated EZH2 axis in oral tongue squamous cell carcinoma. *Oncotarget*. 2015;6(9):6797–6810. doi:10.18632/oncotarget.v6i9
48. Tan YK, Liu KJ, Zou H, et al. Inhibitory effect and molecular mechanism of the new phorphyrin-based HCE6 photosensitizer on the activity of MKN45 human gastric cancer cells. *J Biomed Nanotechnol*. 2019;15(6):1345–1353. doi:10.1166/jbn.2019.2774
49. Xu T, Ding J, Ge H, et al. Effects of VCP979 novel p38 mitogen activated protein kinase inhibitor on progression of pancreatic cancer in mouse model with diabetic conditions. *J Biomed Nanotechnol*. 2019;15(6):1325–1333. doi:10.1166/jbn.2019.2775
50. Fan L, Wang J, Meng F, et al. Delivering the acetylcholine neurotransmitter by nanodrugs as an effective treatment for Alzheimer's disease. *J Biomed Nanotechnol*. 2018;14(12):2066–2076. doi:10.1166/jbn.2018.2649
51. Gao J, Li W, Guo Y, Feng SS. Nanomedicine strategies for sustained, controlled and targeted treatment of cancer stem cells. *Nanomedicine*. 2016;11(24):3261–3282. doi:10.2217/nnm-2016-0261
52. Xie FY, Xu WH, Yin C, Zhang GQ, Zhong YQ, Gao J. Nanomedicine strategies for sustained, controlled, and targeted treatment of cancer stem cells of the digestive system. *World J Gastrointest Oncol*. 2016;8(10):735–744. doi:10.4251/wjgo.v8.i10.735
53. Li R, Wu W, Liu Q, et al. Intelligently targeted drug delivery and enhanced antitumor effect by gelatinase-responsive nanoparticles. *PLoS One*. 2013;8(7):e69643. doi:10.1371/journal.pone.0069643
54. Xu L, Wu S, Zhou X. Bioinspired nanocarriers for an effective chemotherapy of hepatocellular carcinoma. *J Biomater Appl*. 2018;33(1):72–81. doi:10.1177/0885328218772721
55. Podduturi VP, Magana IB, O'Neal DP, Derosa PA. Simulation of transport and extravasation of nanoparticles in tumors which exhibit enhanced permeability and retention effect. *Comput Methods Programs Biomed*. 2013;112(1):58–68. doi:10.1016/j.cmpb.2013.06.011
56. Kim B, Seo B, Park S, et al. Albumin nanoparticles with synergistic antitumor efficacy against metastatic lung cancers. *Colloids and Surfaces B: Biointerfaces*. 2017;158:157–166. doi:10.1016/j.colsurfb.2017.06.039
57. Hingorani DV, Lippert CN, Crisp JL, et al. Impact of MMP-2 and MMP-9 enzyme activity on wound healing, tumor growth and RACPP cleavage. *PLoS One*. 2018;13(9):e0198464. doi:10.1371/journal.pone.0198464
58. Choi JH, Kim H, Kim HS, Um SH, Choi JW, Oh BK. MMP-2 detective silicon nanowire biosensor using enzymatic cleavage reaction. *J Biomed Nanotechnol*. 2013;9(4):732–735. doi:10.1166/jbn.2013.1541
59. Zhu L, Wang T, Perche F, Taigind A, Torchilin VP. Enhanced anticancer activity of nanopreparation containing an MMP2-sensitive PEG-drug conjugate and cell-penetrating moiety. *Proc Natl Acad Sci U S A*. 2013;110(42):17047–17052. doi:10.1073/pnas.1304987110
60. Ke W, Zha Z, Mukerabigwi JF, et al. Matrix Metalloproteinase-responsive multifunctional peptide-linked amphiphilic block copolymers for intelligent systemic anticancer drug delivery. *Bioconjug Chem*. 2017;28(8):2190–2198. doi:10.1021/acs.bioconjchem.7b00330
61. Liu SS, Maguire EM, Bai YS, et al. A novel regulatory axis, CHD1L-MicroRNA 486-matrix metalloproteinase 2, controls spermatogonial stem cell properties. *Mol Cell Biol*. 2019;39(4):e00357–18.
62. Dang Y, Lin Y, Sun H, Sun J, Li C, Li Z. Isoliquiritigenin can inhibit migration and invasion of human glioma stem cells by down-regulating matrix metalloproteinases. *Journal of Zhejiang University. Medical Sciences*. 2018;47(2):181–186.
63. Li F, Dai L, Niu J. GPX2 silencing relieves epithelial-mesenchymal transition, invasion, and metastasis in pancreatic cancer by down-regulating Wnt pathway. *J Cell Physiol*. 2019. doi:10.1002/jcp.29391
64. Wu FL, Li RT, Yang M, et al. Gelatinases-stimuli nanoparticles encapsulating 5-fluorouridine and 5-aza-2′-deoxycytidine enhance the sensitivity of gastric cancer cells to chemical therapeutics. *Cancer Lett*. 2015;363(1):7–16. doi:10.1016/j.canlet.2015.01.006
65. Cui FB, Li RT, Liu Q, et al. Enhancement of radiotherapy efficacy by docetaxel-loaded gelatinase-stimuli PEG-Pep-PCL nanoparticles in gastric cancer. *Cancer Lett*. 2014;346(1):53–62. doi:10.1016/j.canlet.2013.12.002
66. Liu Q, Li RT, Qian HQ, et al. Gelatinase-stimuli strategy enhances the tumor delivery and therapeutic efficacy of docetaxel-loaded poly (ethylene glycol)-poly(varepsilon-caprolactone) nanoparticles. *Int J Nanomedicine*. 2012;7:281–295. doi:10.2147/IJN
67. Liu Q, Li R, Zhu Z, et al. Enhanced antitumor efficacy, biodistribution and penetration of docetaxel-loaded biodegradable nanoparticles. *Int J Pharm*. 2012;430(1–2):350–358. doi:10.1016/j.ijpharm.2012.04.008
68. Liu B, Yang M, Li R, et al. The antitumor effect of novel docetaxel-loaded thermosensitive micelles. *Eur J Pharm Biopharm*. 2008;69(2):527–534. doi:10.1016/j.ejpb.2008.01.015

69. Li R, Li X, Xie L, et al. Preparation and evaluation of PEG-PCL nanoparticles for local tetradrine delivery. *Int J Pharm*. 2009;379(1):158–166. doi:10.1016/j.ijpharm.2009.06.007
70. Zhu Z, Li Y, Li X, et al. Paclitaxel-loaded poly(N-vinylpyrrolidone)-b-poly(ε-caprolactone) nanoparticles: preparation and antitumor activity in vivo. *J Controll Release*. 2010;142(3):438–446. doi:10.1016/j.jconrel.2009.11.002
71. Liu Q, Li RT, Qian HQ, et al. Targeted delivery of miR-200c/DOC to inhibit cancer stem cells and cancer cells by the gelatinases-stimuli nanoparticles. *Biomaterials*. 2013;34(29):7191–7203. doi:10.1016/j.biomaterials.2013.06.004
72. Yao C, Cao X, Fu Z, et al. Boschniakia rossica polysaccharide triggers laryngeal carcinoma cell apoptosis by regulating expression of Bcl-2, Caspase-3, and P53. *Med Sci Monitor*. 2017;23:2059–2064. doi:10.12659/MSM.901381
73. Guestini F, Ono K, Miyashita M, et al. Impact of Topoisomerase IIalpha, PTEN, ABCC1/MRP1, and KI67 on triple-negative breast cancer patients treated with neoadjuvant chemotherapy. *Breast Cancer Res Treat*. 2018;173:275–288.
74. Chaffer CL, Marjanovic ND, Lee T, et al. Poised chromatin at the ZEB1 promoter enables breast cancer cell plasticity and enhances tumorigenicity. *Cell*. 2013;154(1):61–74. doi:10.1016/j.cell.2013.06.005
75. Chen D, Yu D, Wang X, et al. Epithelial to mesenchymal transition is involved in ethanol promoted hepatocellular carcinoma cells metastasis and stemness. *Mol Carcinog*. 2018;57(10):1358–1370. doi:10.1002/mc.v57.10
76. Fan M, Sethuraman A, Brown M, Sun W, Pfeffer LM. Systematic analysis of metastasis-associated genes identifies miR-17-5p as a metastatic suppressor of basal-like breast cancer. *Breast Cancer Res Treat*. 2014;146(3):487–502. doi:10.1007/s10549-014-3040-5
77. Huang RY, Guilford P, Thiery JP. Early events in cell adhesion and polarity during epithelial-mesenchymal transition. *J Cell Sci*. 2012;125(Pt 19):4417–4422. doi:10.1242/jcs.099697
78. Xavier PLP, Cordeiro YG, Rochetti AL, et al. ZEB1 and ZEB2 transcription factors are potential therapeutic targets of canine mammary cancer cells. *Vet Comp Oncol*. 2018;16:596–605. doi:10.1111/vco.2018.16.issue-4
79. Lee HM, Hwang KA, Choi KC. Diverse pathways of epithelial mesenchymal transition related with cancer progression and metastasis and potential effects of endocrine disrupting chemicals on epithelial mesenchymal transition process. *Mol Cell Endocrinol*. 2017;457:103–113. doi:10.1016/j.mce.2016.12.026